Contactless Battery Charger Controller for Wireless Sensor Node

Róger W. P. da Silva, Valner Brusamarello,
Diego Eckhard, Carlos E. Pereira, João C. Netto
Federal University of Rio Grande do Sul – UFRGS
Porto Alegre, Brazil
{roger.willian, valner.brusamarello, diegoeck}@ufrgs.br,
cpereira@ece.ufrgs.br, netto@inf.ufrgs.br

Ivan Müller
State University of Rio Grande do Sul – UERGS
Guaíba, Brazil
ivan-muller@uergs.edu.br

***Abstract*—Wireless sensor network nodes have been used to collect data from processes in several different areas. In most cases, these sensors and their batteries need to be recharged regularly. However, these sensors are often deployed in harsh environments that can damage them with moist and dust particles. Therefore this work aims to present a contactless inductive charger developed to avoid jack or plug holes on the sensor casing in order to prevent damage to its circuitry. This battery charger uses a resonant topology circuit and an algorithm to adjust the resonant frequency. Unlike a previous work, it measures the current through the primary coil to determine the optimal point, which yields a simpler solution. The concept has been proven to be effective while keeping low cost and simplicity, which are important aspects to wireless sensor networks.**

***Keywords*—wireless sensor network, wireless power transfer, battery charger, optimization algorithm.**

I. Introduction

Small sized remote sensing devices that include wireless communication can be used to collect data and assist in various application areas. However, these devices may have particular needs regarding power and robustness against environmental conditions.

These small sensing devices are generally low power, battery powered devices, whose batteries will inevitably discharge. If these are primary (non-rechargeable) batteries, they will need to be replaced or, if they are secondary, will need to be recharged. In both cases, some kind of circuit is usually exposed (jacks, plugs or contacts) and that compromises the sensor node robustness against environmental conditions.

To deal with these problems to prolong the sensor lifetime, it is necessary to improve the power supply system, which includes longer periods between charges and employing an alternative way to transfer power to devices. Battery endurance is constantly being increased by lowering the power consumption of the circuits and improving the battery chemicals. Therefore, this work presents a simple circuit and algorithm to deliver wireless power to recharge a sensor node's battery, allowing an airtight node enclosure.

The proposed contactless battery charger makes use of resonant inductors and capacitors whose driver's frequency is on-line adjusted by the algorithm to maximize power transfer. The inductors, which are the energy transfer coils, are placed less than 10 mm apart from each other (empirical observation), one in the sensor and the other in the data collector device, which is chosen to be the wireless power source. This work uses an approach that differs from a previous one [1] by measuring the current that flows through the primary driver to determine the resonance frequency, without a radio link or any other type of communication. When the system is operating at this frequency, the amount of power trasferred to the secondary is increased.

Moreover, the devices employed to verify this solution used to be recharged through a mini-USB port, which is inappropriate for harsh environment applications, such as precision agriculture and livestock. Therefore, this work increases the device's endurance widening its application field.

The remainder of this paper is organized as follows: In Section II are presented related works that represent the context in which this work fits. In Section III, the methodology that was used for the development of a wireless battery charger is presented. In Section IV the developed battery charger, the experiments and results are presented. Finally, conclusions and future works are shown in Section V.

II. Related Works

Wireless sensor networks (WSN) have attracted increasing attention in the last years, especially because they potentiate internet of things. In this context many works have been published presenting applications related to large data collection and their use in many research areas. Some examples include small, mobile, and remote sensing devices used in wearable computing and human body monitoring [2], perishable goods [3], precision agriculture [4], fire detection in forests [5], to name a few.

The process employed to transfer power wirelessly (wireless power transfer, WPT), has been studied since the beginning of the last century and is well known today. This process is well established and has been used in low power biomedical implants such as cochlear [6]. However, this subject regained attention since the ability to transfer energy wirelessly at considerable distances by means of inductive coupling with resonating coils was demonstrated [7].

In the context of wireless sensor networks, WPT has been studied with various objectives, such as increasing availability of energy for specific network nodes [8], [9], to recharge sensor batteries [10], or even replace them completely [11].

One of the challenges of WPT is to achieve an amount of transferred power that permits its practical employment to power the remote device. As previously mentioned, this can be achieved with resonant coils and capacitors and operating at the necessary resonant frequency to maximize energy transfer. In [1] the authors propose the employment of RF wireless links to establish a closed loop control in order to adjust the oscillator frequency to reach resonance, thus maximizing the inductive coupling. Another possibility is to use simultaneous modulation over the inductive link with the purpose to send control data back to the charger to tune the oscillator, as presented in [6]. These two approaches present drawbacks such as more complex circuits to modulate/demodulate or energy wasting to power the radio link. Therefore, this work presents an enhancement of the solution proposed in [1], in the sense that the communication between the wireless power station and the sensor node are no longer needed, simplifying the circuit and saving energy. Another advantage brought by this approach is the possibility of recharging a node whose battery is completely discharged, since the node does not need to be on to charge the battery. The proposed solution is developed and verified using real multi-purpose WSN nodes called Namimotes [12].

III. Methodology

The WPT system presented here is divided into two parts for better comprehension: a power transmission module, inside the charger, and the power receiving module, that is part of sensor node to be recharged.

The power transmission module comprises a circuit for power transmission and a control unit, where the algorithm for the resonance frequency search is executed. Figure 1 shows the components of the power transmission module. It comprises a power source that provides energy to the entire system, a driver (and controller) to supply current to the coil, and a low power oscillator whose frequency is controlled by the control unit. This module is assembled on top of the collector node's hardware, this way its microcontroller unit (MCU) is used to tune the driver's oscillator. Although this is not necessary, this approach leverages the collector's hardware that would otherwise be underused.

The receiving module is composed by the secondary coil, a low drop rectifier, a voltage regulator, and a circuit that controls the battery charging process. This module is part of the sensor node's circuits.

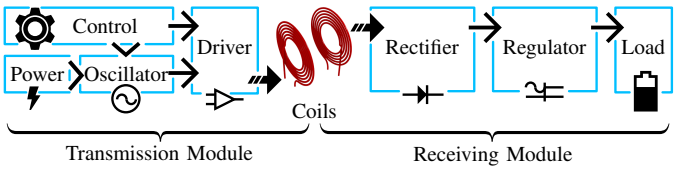

Fig. 1. Wireless power transfer system.

A. Control Unit

The collector node employs a MC13224 MCU where the control algorithm runs, since it also constitutes the control unit hardware as mentioned above. The control algorithm searches for the tuning frequency of the circuit, compensating misalignments in the relative position of the coils, as well as variations such as temperature drifts or aging. The position misalignments constitute the main cause of changes in the resonance frequency and coupling factor.

B. Low-Power Oscillator

One of four programmable counter blocks within the MCU hardware composes the core of the low power oscillator. This block is set up to count on every edge of the system clock and to generate a square wave signal whose period is related to a programmable overflow value. This signal is routed to drive an output pin of the MCU. Since the system clock has a frequency of 24 MHz the square wave frequency is given by (1), where n is a 16-bit unsigned integer overflow value loaded into the counter register.

$$f_{osc} = \frac{12 \times 10^6}{n} \quad \text{(Hz)} \tag{1}$$

By using the collector's MCU and its internal timers to control the coils frequency, the use of additional hardware is eliminated, leading to a more compact circuit and cost reduction.

C. Primary Coil Driver

A MAX 256 integrated circuit is chosen to be the coils driver because its internal H-bridge topology is very suitable to this application. This driver has under-voltage lockout protection, thermal protection, and a watchdog to monitor and prevent continuous current to flow through the coil. The MCU timer output pin is connected to the driver's input and the driver's output is connected directly to the coil. No impedance adapters between the driver and the coil are needed.

The MAX 256 divides the reference input frequency by two, which leads to the following equation for the frequency at the primary coil:

$$f_{coil} = \frac{6 \times 10^6}{n} \quad \text{(Hz)} \tag{2}$$

The resonance frequency for the developed circuit lies between 100 and 200 kHz, therefore, accordingly to (2), n must assume a value between 30 and 60.

A 0.02 Ω shunt resistor is placed in series with the driver circuit to permit the acquisition of the value of the current that flows through the driver. An AC component is observed in the shunt voltage because of the coil inductance, therefore the signal must be rectified before sampling. The DC value of the current, measured through the voltage across the shunt resistor, feeds the resonance search algorithm.

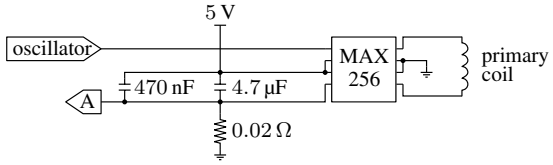

Fig. 2. Primary coil driver.

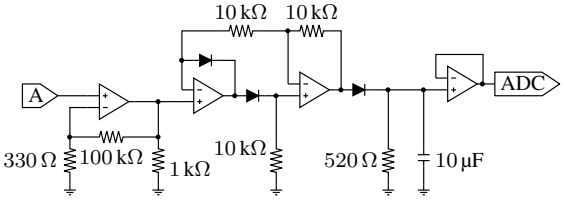

Fig. 3. Instrumentation circuit.

Figure 2 shows the driver circuit along with the shunt resistor. The shunt voltage signal is conditioned by the circuit in Fig. 3, which amplifies, rectifies and holds its the peak value during the MCU's ADC acquisition time.

D. High-Frequency Coils

Two commercial planar coils shown in Fig. 4 are employed: the primary is a circular-shaped Litz wire coil, while the secondary has an oblong format and is made of regular wire.

The primary coil's circular shape provides a greater freedom to position it in relation to the secondary, reducing the impact on the coupling factor between the coils. The secondary coil has an oblong shape and dimensions compatible with the housing of the sensor node. Since the coils are located very close to the other circuits, they both have a ferrite plate whose main role is to shield the circuits from the electromagnetic field variations.

The amount of power that reaches the battery charging circuit is impacted by the losses that occur in the coils, due to the skin and proximity effects, and by the small coupling factor [13]. These losses are reduced by using the correct coils and by adding parallel capacitors with the secondary coil for the system to operate in resonance [1]. However, when using capacitors to put the system in resonance, the capacitor losses must also be taken into account. Therefore the capacitors must present low equivalent series resistance (ESR). Besides, the skin effect has an increased influence on higher frequencies, then the system components are chosen in a way that the resonance frequency is well bellow 1 GHz.

Another factor that must be taken into consideration is the distance between the coils. Since this is a low power transmission system and the coils are small, the distance between them must be as reduced as possible, limited only by the node enclosure thickness. Therefore, to achieve a practical power value at the load, it is expected that the secondary coil is no farther than 10 mm from the primary coil when the battery is charging.

E. Voltage Rectifier

Because the power reaching the voltage rectifier is relatively low, its components must present low losses. Thus, a bridge rectifier composed by Schottky diodes, with low voltage drop and high switching frequency is employed here.

F. Voltage Regulator

The voltage regulator maintains a constant voltage that powers the battery charging and other sensor node's circuits. When there is little load on the secondary (i.e. when the battery is fully charged), the voltage over the terminals of the coil tends to rise, so the voltage regulator must also withstand high voltages at the input. Therefore the circuit employs an automotive voltage regulator which supports voltages up to 45 V. The regulator's nominal output voltage is 5 V with 2 % of regulation.

G. Load

The load presented to the receiver circuit is the battery charging circuit that already exists in the sensor node. The whole recharge process is managed by a MAX 1811, an integrated circuit specifically designed for this task. The battery used in Namimote is a Li^+ cell type battery that can be recharged using a current of 100 or 500 mA.

In order to simulate the battery charging circuit, the power receiving circuit is connected to a resistor. Because the output of the voltage regulator is little more than 5 V, a 50 Ω resistor is connected to allow a current of approximately 100 mA. Figure 5 shows the secondary coil on the power receiving circuit: it can be observed the resonant capacitors (C22 at the PCB) and the resistive load that simulates the battery charging circuit.

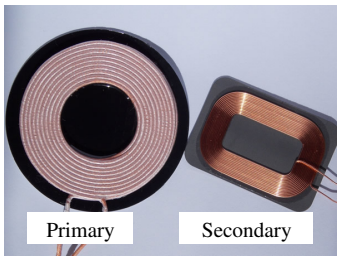

Fig. 4. Primary and secondary coils.

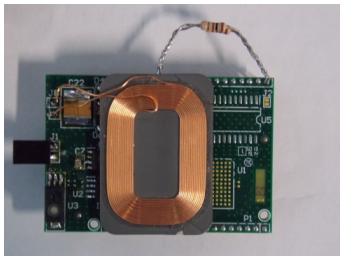

Fig. 5. Power receiving circuit.

```
1: defcnt ← 60 {initial frequency=100 kHz}
2: defstep ← −1
3: min ← 30
4: max ← 60
5: thresh ← 400
6: loop
7:    n ← defcnt
8:    last ← 0
9:    step ← defstep
10:   repeat
11:      read current
12:      if current < last then
13:         step ← −step
14:      end if
15:      n ← n + step
16:      last ← current
17:      wait 200 ms
18:   until current < thresh or n < min or n > max
19: end loop
```

Fig. 6. Hill-climbing algorithm that searches the resonance frequency.

H. Resonance Search Algorithm

A very simple search algorithm based on the method of optimization known as hill-climbing is developed to adjust the frequency of the system in order to achieve resonance. The algorithm simplicity makes its implementation straightforward but also helps to keep the processing load low and save energy at the wireless charging station.

This method consists of starting at some initial point, assess the value of the function to be optimized in that point's neighborhood, if verified that there is a better point (considering the function values), continue the search from there.

Figure 6 shows the pseudo code of the algorithm implemented. The algorithm starts the search at a particular frequency, e.g. 100 kHz, or $n = 60$, according with (2). Then the frequency is increased (n is decremented) and the current value is read by the MCU's ADC. If there is an improvement, the search continues in this direction, otherwise the direction of frequency changing is reversed.

The time between each iteration is set to 200 ms, so the algorithm is also fast since it would take at most 6 seconds to find the resonance in the worst case, which is to sweep all the allowed frequencies.

Apart from exceptional situations, the algorithm is always looking for another resonance frequency. Therefore instead of stopping at the resonance frequency, it maintains the frequency of coils in the surroundings of this optimal region. This approach has the advantage that the new resonance frequency will be promptly found in the event of a significant change in the system parameters, i.e. when the coupling changes or the battery is fully charged. It also helps to keep the algorithm simple.

In case the driver current falls below the desired threshold or the frequency is out of stipulated limits, the algorithm is restarted with its default initial values.

IV. Results

To validate the proposal, the wireless energy transmission circuit is assembled, and connected to the Namimote network collector node. The receiving circuit is mounted with a resistive load as shown in Fig. 5. Then the receiver is positioned over the primary coil circuit and four experiments are conducted.

The first experiment aims to verify that the algorithm finds the optimal point regardless the initial frequency chosen. The second and third experiments check that the system finds the resonance frequency for different coil positions. Finally, the last one aims to find the relation between the power delivered to the load and the power delivered to the driver and to identify the point where the power delivered is maximum.

The exact positions of the coils are omitted, since they are not relevant to any of the experiments as long as the coils are close enough to reach the resonance. Therefore the coils are positioned parallel to each other, the distance between the coil planes is kept within a 10 mm range and the coil centers are misaligned up to 5 mm along the same planes.

During the first experiment the coils are maintained at the same position and the experiment is conducted with the algorithm starting at two opposite frequencies.

The results are in Fig. 7, that shows the evolution of the input signal (n), and the output signal (ADC value) along the algorithm iterations. Although starting at two opposite frequencies for the same position of the coils, the algorithm has found the same resonance frequency, which is around 125 kHz ($n = 48$). It is easy to see that when the resonance is reached the output curves are no longer monotonic, indicating a local maximum. The circuit parameters are chosen in order to keep the global maximum as the sole maximum within the allowed frequency range.

Once defined that the algorithm can operate properly regardless of the starting frequency, the second experiment is carried out to determine if the system is capable of finding the resonance frequency for different coil positions.

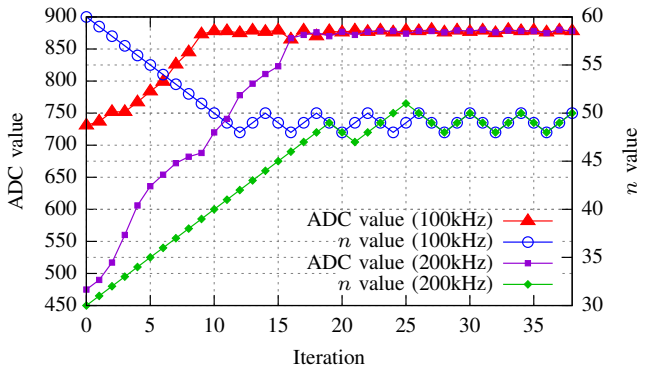

Fig. 7. Iterative response for the same coil position and two distinct initial frequencies (within parenthesis).

First, the algorithm starts at 100 kHz ($n = 60$) and five arbitrary positions are verified.

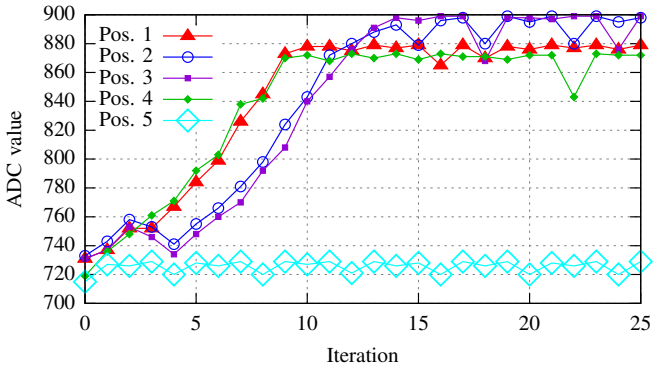

Fig. 8. Current evolution for five arbitrary coil positions and starting at 100 kHz ($n = 60$).

Figure 8 shows the evolution of the output signal along the algorithm iterations the resonance. Different positions yield different coupling factors which, in turn, yield different current values. For position 5 it converges immediately.

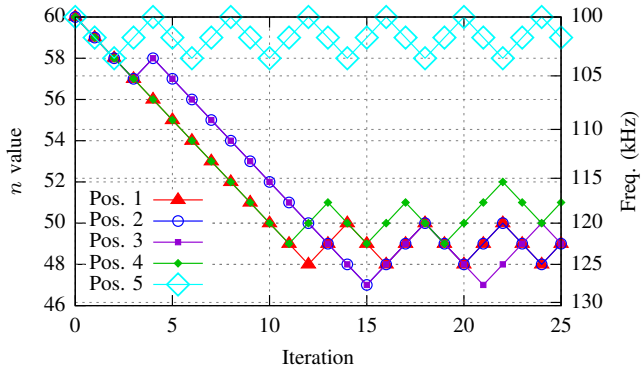

Fig. 9. Frequency evolution for the same five positions and starting at 100 kHz ($n = 60$).

Figure 9 shows the evolution of the input signal n and the respective frequencies along the algorithm iterations for each position. Each position results in a different resonance frequency, which the algorithm is able to find. For each position the algorithm is able to find a respective resonant frequency at which the current flowing is maximum, which is proven by the current drop that occurs if the frequency varies in any direction.

Then the experiment is repeated with five other arbitrary positions, but this time with the algorithm starting the search at the highest frequency (200 kHz or $n = 30$).

The evolution of the output signal during this experiment is shown in Fig. 10. The results are similar to those of the previous experiment: the resonance is reached when the current through the primary driver cannot be further increased. For each position the system is able to reach the resonance.

Figure 11 shows the evolution of the input signal n and the respective frequencies throughout the iterations of the

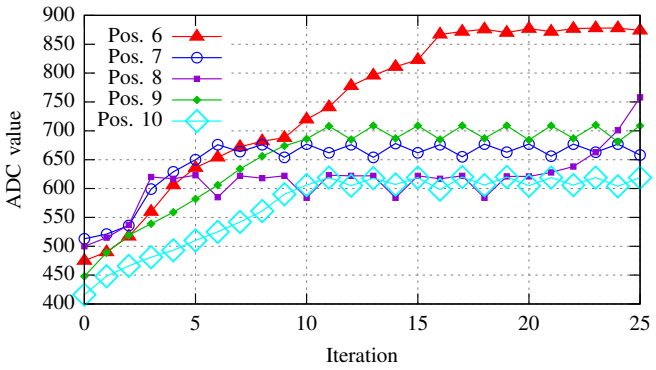

Fig. 10. Current evolution for other five arbitrary coil positions and starting at 200 kHz ($n = 30$).

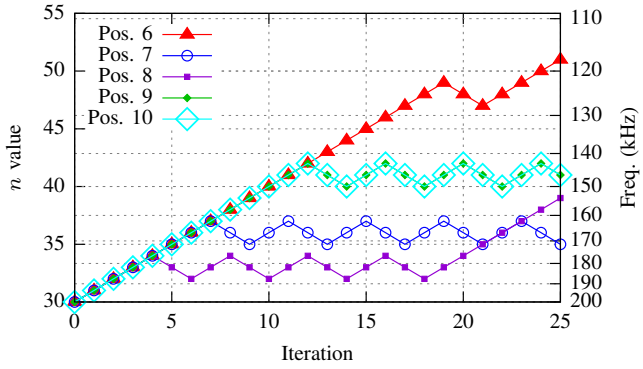

Fig. 11. Frequency evolution for the same five positions and starting at 200 kHz ($n = 30$).

algorithm. Again, for each different coil position a different resonance frequency is observed, and the algorithm is capable of finding it.

The results show that, regardless of the initial frequency, the algorithm operates as expected for various coil positions. That is, it is able to find the frequency at which the current reaches its maximum value.

The last experiment is carried out in order to check the overall efficiency of the system, with the aim to determine the feasibility of using it to recharge a real battery in Namimote sensor node. Therefore, an ammeter is connected in series with the primary coil driver and a voltmeter in parallel with the resistive load simulating the battery in charging process. Then, the WPT system is put into operation with the coils in several different arbitrary positions. For each position, after the system accommodates (i.e. the resonance frequency is found), the values are recorded.

The obtained values for the current and the voltage in the driver, and current in the resistive load are presented in Fig. 12. Each point results from a different resonance frequency caused by a different coil position. The horizontal line is the maximum value of load voltage limited by the voltage regulator. The oblique straight line is a linear fitting of the points until the regulation region.

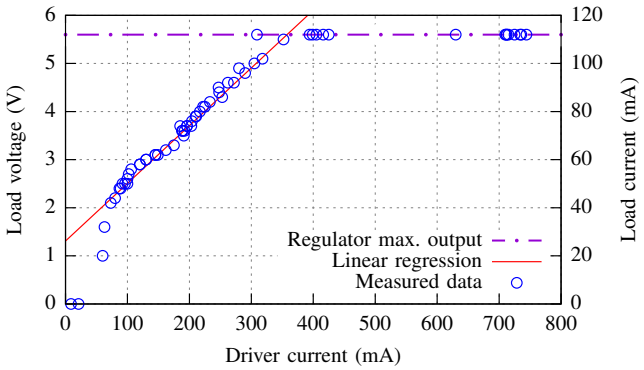

Fig. 12. Load voltage and current vs. driver current for several arbitrary coil positions.

According to the linear fitting result, when the system is close to the resonance before the regulation region, the voltage over the load is approximated by (3):

$$V_{load} = 1.308 + 12 \times I_{driver} \qquad \text{(V)} \tag{3}$$

Also, since the load is $50\,\Omega$, the current through the load is given by (4) below.

$$I_{load} = 26.16 + 240 \times I_{driver} \qquad \text{(mA)} \tag{4}$$

Not all points represent good points of operation, the optimal region of operation is around the point of intersection of the two lines in the plot of Fig. 12. At this point the current through the load is maximum and yet there is no waste of energy on the regulator. During the experiment, the voltage on the driver is always maintained at $5\,\text{V}$ and at this point the voltage across the load is $5.6\,\text{V}$, the current in the driver is about $358\,\text{mA}$ and the load current is approximately $112\,\text{mA}$.

Under these conditions, the power delivered to the driver is approximately $1.79\,\text{W}$ and the power delivered to the load is approximately $627.2\,\text{mW}$. Therefore, the efficiency of the WPT system in this scenario is about $35\,\%$ and the energy delivered to the load is more than enough to power the battery recharging process with the considered sensor node.

V. Conclusions

This paper presents a wireless battery charger for recharging the battery of a WSN node. The development of this charger allows subsequent development of a watertight housing for the sensor node, which is desirable for most of practical applications. The developed solution delivered enough power for the battery recharging process.

To achieve that, the system is allowed to resonate through the use of high frequency coils and capacitors. A simple algorithm was employed to find the system resonance frequency when it is operating, because the resonance frequency depends on the coils position. This algorithm tries to maximize the value of the current flowing through the driver of the primary coil adjusting the frequency. This approach simplifies the circuit topology compared with other common approaches, that use communication links between the charger station and the charging node in order to adjust the frequency. This led to a simpler, more robust and cost-effective solution.

Experiments were conducted to verify that the system operates properly, considering different positions of the coils and different initial frequencies. The obtained results showed that the presented system is feasible and is able to transfer sufficient power to feed the battery recharging process when the system is at resonance. The developed algorithm is capable of finding the resonance frequency, regardless of the initial conditions (coil positioning, starting frequency, remaining load, etc.). As a future work a further analysis of individual efficiency of system components is intended to find possible points of improvement.

References

[1] V. J. Brusamarello, Y. B. Blauth, R. Azambuja, and I. Muller, "A study on inductive power transfer with wireless tuning," in *2012 IEEE International Instrumentation and Measurement Technology Conference (I2MTC) Proceedings*, vol. 1, 2012 IEEE International Instrumentation and Measurement Technology Conference. New York: IEEE, 2012, pp. 1098–1103.

[2] B. Rahul Nandkishor, A. Shinde, and P. Malathi, "Android smartphone based body area network for monitoring and evaluation of medical parameters," in *Networks & Soft Computing (ICNSC), 2014 First International Conference on*. IEEE, pp. 284–288.

[3] V. F. Annese and D. D. Venuto, "On-line shelf-life prediction in perishable goods chain through the integration of wsn technology with a 1st order kinetic model," in *Environment and Electrical Engineering (EEEIC), 2015 IEEE 15th International Conference on*. IEEE, pp. 605–610.

[4] G. H. E. L. De Lima, L. C. E. Silva, and P. F. R. Neto, "Wsn as a tool for supporting agriculture in the precision irrigation," in *Networking and Services (ICNS), 2010 Sixth International Conference on*. IEEE, 2010, pp. 137–142.

[5] Z. G. Kovács, G. E. Marosy, and G. Horváth, "Case study of a simple, low power wsn implementation for forest monitoring," in *Electronics Conference (BEC), 2010 12th Biennial Baltic*. IEEE, 2010, pp. 161–164.

[6] K. Van Schuylenbergh and R. Puers, *Inductive Powering Basic Theory and Application to Biomedical Systems*. Dordrecht: Springer, 2009.

[7] A. Kurs, A. Karalis, R. Moffatt, J. D. Joannopoulos, P. Fisher, and M. Soljačić, "Wireless power transfer via strongly coupled magnetic resonances," *Science*, vol. 317, no. 5834, pp. 83–86, June 2007.

[8] T. He, K.-W. Chin, and S. Soh, "On using wireless power transfer to increase the max flow of rechargeable wireless sensor networks," in *Intelligent Sensors, Sensor Networks and Information Processing (ISSNIP), 2015 IEEE Tenth International Conference on*. IEEE, 2015, pp. 1–6.

[9] M. Pan, H. Li, Y. Pang, R. Yu, Z. Lu, and W. Li, "Optimal energy replenishment and data collection in wireless rechargeable sensor networks," in *Global Communications Conference (GLOBECOM), 2014 IEEE*. IEEE, 2014, pp. 125–130.

[10] G. P. Hancke and N. Vorster, "The feasibility of using resonant inductive power transfer to recharge wireless sensor network nodes," in *Wireless Power Transfer Conference (WPTC), 2014 IEEE*. IEEE, 2014, pp. 100–105.

[11] L. Angrisani, F. Bonavolontà, G. d'Alessandro, and M. D'Arco, "Inductive power transmission for wireless sensor networks supply," in *Environmental Energy and Structural Monitoring Systems (EESMS), 2014 IEEE Workshop on*. IEEE, 2014, pp. 1–5.

[12] I. Müller, E. P. d. Freitas, A. A. Susin, and C. E. Pereira, "Namimote: A low-cost sensor node for wireless sensor networks," in *Internet of Things, Smart Spaces, and Next Generation Networking*, ser. Lecture Notes in Computer Science. Heidelberg: Springer, 2012, vol. 7469, pp. 391–400.

[13] W. G. Hurley and W. H. Wölfle, *Transformers and inductors for power electronics: theory, design and applications*. Hoboken: Wiley-Blackwell, 2013.